


Uncovering the spatial distribution of stars and dust in $z \sim 2$ Submillimeter Galaxies

Philipp Lang¹ , Eva Schinnerer¹, Ian Smail², U. Dudzevičiūtė²,
A. M. Swinbank² and the A3COSMOS,
AS2UDS and ALESS Teams

¹Max-Planck-Institut für Astronomie, Königstuhl 17, D-69117 Heidelberg, Germany

²Center for Extragalactic Astronomy, Department of Physics, Durham University,
South Road, Durham DH1 3LE, UK

Abstract. The spatial distribution of the dust and stars contains crucial information about the evolutionary pathways of galaxies. We present results of our study combing high-resolution ALMA and HST observations of $z \sim 2$ bright sub-millimeter galaxies (SMGs). We have developed a two-dimensional extinction and age correction technique to obtain accurate stellar mass distributions from HST/CANDELS. For the first time, we can directly compare the spatial distribution of assembled stellar mass and ongoing star formation on kpc scales for distant SMGs, shedding light on their highly debated formation mechanisms. We find that the dust distribution is more compact than the stellar component, regardless if the SMG lies on the main sequence or at the starburst regime. Taking the dust emission as a proxy for dust-obscured star formation, our results imply that high-redshift SMGs are experiencing centrally enhanced star formation. These findings suggests that major galaxy interactions are not necessarily the main formation channel for SMGs with secular disk formation remaining a viable option as suggested by state-of-the-art cosmological simulations. The sizes and stellar densities of our $z \sim 2$ SMGs agree well with the most compact early-type galaxies in the local Universe, strongly supporting the idea that the latter systems are indeed the descendants of massive SMGs at $z \sim 2$.

Keywords. galaxies: evolution, galaxies: high-redshift, galaxies:structure, submillimeter

1. Introduction

The brightest class of IR-luminous galaxies, detected with single-dish sub-mm/mm surveys (therefore dubbed sub-mm galaxies, ‘SMGs’), are associated with the highest SFRs ($> 300 M_{\odot}/\text{yr}$) and IR luminosities ($L_{\text{IR}} > 10^{12} L_{\odot}$). Since they contribute a significant fraction to the total star formation rate density ($\sim 10\text{-}30\%$; e.g., Swinbank *et al.* 2014) and are thought to be the progenitors of today’s massive ellipticals (e.g., Swinbank *et al.* 2006; Ikarashi *et al.* 2015), it is crucial to understand their evolutionary paths in the early Universe. In our canonical picture, the general star-forming population of galaxies on the star-forming main sequence evolves through cold gas accretion (e.g., Dekel *et al.* 2009), while SMGs represent merger-induced and short-lived starbursts (e.g., Narayanan *et al.* 2010). However, theoretical models suggest that distant SMGs are simply the high-mass extension of non-interacting galaxies where star formation is triggered through the slower internal secular processes (e.g. Hayward *et al.* 2011, 2013).

Recent studies based on ALMA (e.g. Simpson *et al.* 2015a; Hodge *et al.* 2016; Tadaki *et al.* 2017a) have revealed compact sub-mm dust cores (with effective radii of $R_e \sim 1\text{-}2$ kpc) in SMGs at $z \sim 1\text{-}5$. Using the dust continuum as a proxy for massive star formation (i.e. tracing the dust heated by young, massive stars) implies that distant

IR-luminous systems host strong central dust-enshrouded star formation. In contrast, the stellar continuum light morphologies at $z \sim 1-3$ – accessible through high-resolution HST observations – are found to be clearly more extended ($R_e \sim 4-5$ kpc), irregular, as well as spatially decoupled from the FIR/submm emission (e.g., [Chen et al. 2015](#); [Hodge et al. 2016](#)).

These properties are widely associated with a major-merger scenario, in which dissipative collapse of gas causes central star-formation, while the stellar distribution remains in an extended and perturbed configuration. However, there is yet no consensus towards a secular versus major merger origin of SMGs in the literature since the rest-frame optical emission mostly fails to approximate the underlying stellar distribution due to large spatial variations in age and/or extinction, with the latter being most extreme in SMGs with strong central dust obscuration. In this study, we investigate the formation mechanisms of SMGs by combining information on the resolved distribution of both the dust-obscured star formation and the assembled stellar mass on kpc scales. The latter is inferred from the deep multi-wavelength imaging from the CANDELS survey. The results of this study are published in [Lang et al. \(2019\)](#); below, we briefly summarize the method and results.

2. Sample and Method

For our analysis, we construct a sample of 20 SMGs that have been targeted with deep, high angular-resolution observations from both ALMA and *HST* across three cosmological deep fields. We consider submm sources detected in the following surveys: (1) The ALMA-SCUBA-2 Ultra Deep Survey, henceforth referred to as ‘AS2UDS’ ([Stach et al. 2018](#)), (2) ALMA Band 7 follow-up of single-dish submm sources from the LESS survey (‘ALESS’, [Hodge et al. 2013, 2016](#)), and (3) ALMA Band 6 (1.3 mm) follow-up of bright AzTEC sources in the COSMOS field ([Miettinen et al. 2017](#)). Then, we apply the following selection criteria: (a) a redshift range of $1.7 < z < 2.6$, where our method to derive stellar-mass maps is most robust; (b) coverage by *HST*/CANDELS ([Koekemoer et al. 2011](#); [Grogin et al. 2011](#)), and that are detected with sufficient S/N in both J_{125} and H_{160} band filters; (c) no evidence for a central AGN component.

Those yield a final sample of 20 SMGs across a large dynamic range of submm brightness, stellar mass, SFR, and offset from the main sequence. Those properties are further presented in [Figure 1](#), demonstrating that our sample is well representative for the bright and massive SMG population at redshift 2. We note that our selection limits our analysis to systems with bright optical counterparts ($K_s \lesssim 22.9$) due to the requirement of a detection in the *HST* *H* and *J* bands. We derive spatially resolved stellar mass distributions inferred from $J_{125} - H_{160}$ color maps as this filter combination probes rest-frame optical wavelengths at $z \simeq 2$ and can therefore be used to infer stellar M/L ratios. Based on synthetic galaxy SEDs from [\(Bruzual & Charlot 2003\)](#) models, we calibrate a relation between the observed optical M/L ratio and the $J_{125} - H_{160}$ color, that show a robust correlation which is independent of details of the SFH, metallicity and extinction.

3. Results

[Figure 2](#) shows the H_{160} -band cutouts, $J - H$ color maps, and resulting stellar mass maps for a few example cases. Overall, we find that our sources exhibit systematic radial color gradients (i.e. redder centers vs. bluer outskirts). In some cases, off-centered clumps dominating the light distribution in H_{160} -band (such as for ALESS067.1) but only weakly contribute to the stellar mass density. Moreover, the stellar mass distribution of ALESS079.2 appears as a large system with a smooth and strongly centrally peaked mass profile, rather than being comprised of several components as the H_{160} -band image suggests. Those cases highlight the caveat of interpreting highly disturbed rest-frame optical

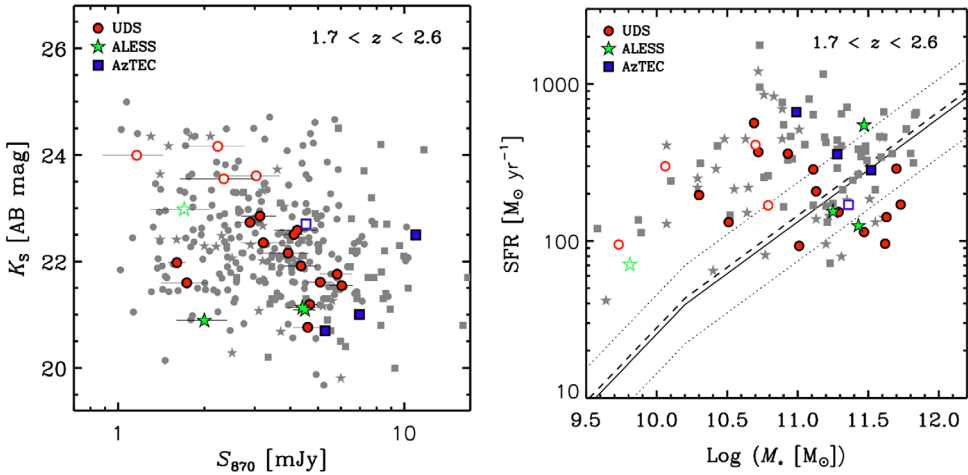


Figure 1. Properties of our SMG sample. Left: K_s -band magnitude versus observed flux density at $870\ \mu\text{m}$. Right: Our SMG sample shown in the M_* -SFR plane. Both quantities are based on SED-derived values from MAGPHYS. Gray symbols show the parent samples of all AS2UDS, ALESS, and AzTEC SMGs in the redshift range $1.7 < z < 2.6$. Filled colored symbols represent our final SMG sample. In addition, open colored symbols identify targets rejected due to their low surface brightness in the *HST*/WFC3 J and H -band imaging. The solid and dotted lines represent the main sequence at redshift 2 (Whitaker *et al.* 2014) and its scatter, respectively.

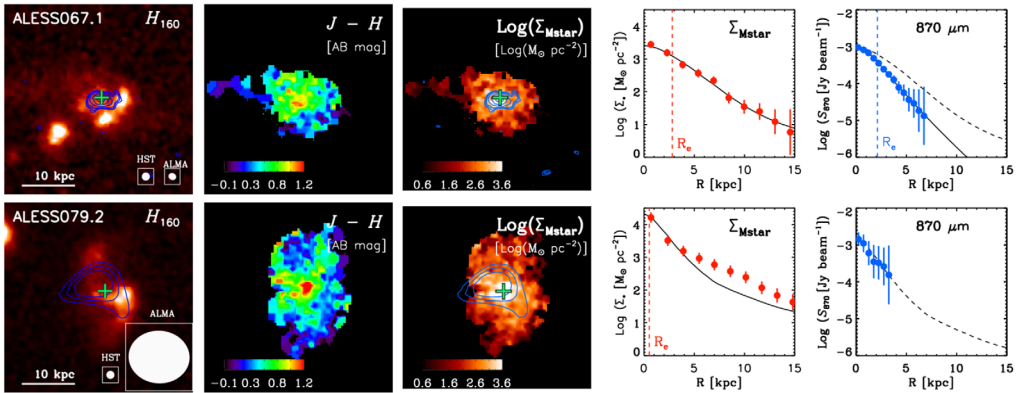


Figure 2. Example cases of our SMG sample; From left to right: H_{160} -band cutouts; $(J_{125} - H_{160})$ color maps; stellar-mass distributions (all with ALMA emission as blue contours); radial stellar mass; and far-infrared ALMA profiles for our SMG sample. Solid lines show our best-fit GALFIT models to the radial profiles. Best-fit mass model re-normalized to the peak of the best-fit submm profile are shown as solid lines.

morphologies commonly seen in SMGs (e.g., Chen *et al.* 2015; Hodge *et al.* 2016). The implied radial trends of M/L within our sources are either caused by variations of stellar age and/or the effects of extinction. With the ALMA/submm emission peak coinciding well with the location of strong color variations, the redder colors are likely the effect of increased extinction towards stronger dust-obscured regions.

As a consequence of the spatial M/L variations, our mass maps show more compact and smoother distributions than the optical images. For the majority of our targets, we confirm that the that stellar mass components are systematically smaller than those of the H_{160} -band light by measuring a median ratio of $\langle R_{e,\text{mass}}/R_{e,H160} \rangle = 0.5 \pm 0.1$.

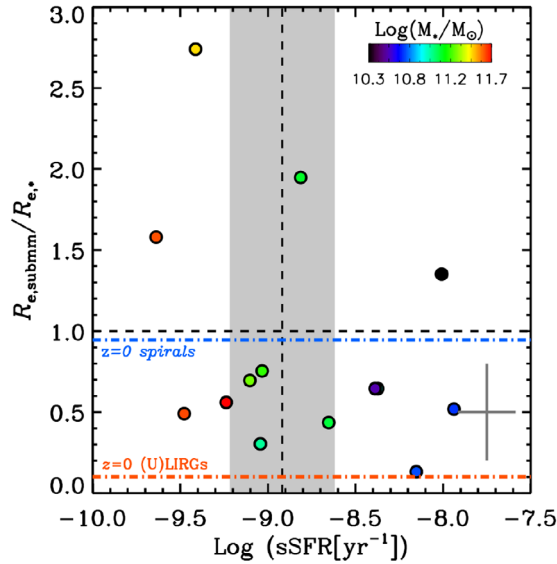


Figure 3. Ratio between intrinsic sizes of the submm and stellar components versus specific star-formation rate, with the color-coding indicating the total stellar mass. The position and scatter of the main sequence, adopted from Whitaker *et al.* 2014, is shown as the dashed vertical line and shaded area, respectively. The colored horizontal lines indicate the median size ratios for local spirals based on KINGFISH sample (Hunt *et al.* 2015), as well as for local (U)LIRGs as based on the GOALS survey (Kim *et al.* 2013). Median uncertainties in the shown properties for our sample are indicated.

We furthermore correlate the inferred size difference between the dust and stellar distributions with the specific star-formation rate, revealing no significant trend (Figure 3). To interpret our observations, we use the dust emission as a tracer of dust-obscured star formation in these systems, relying on the assumption that the dust properties (e.g., dust temperature) do not strongly vary spatially. This points to a picture in which the star formation is clearly more compact than the stellar distribution in high-redshift star-forming galaxies over a large range of specific star-formation rate. Our SMGs exhibit a more compact dust distribution relative to the stars compared to local spiral galaxies, where the dust and stars exhibit an about equal extent. As major interactions can (at least in the local universe) be attributed to the local (U)LIRG population that exhibit very compact dust configurations and large main sequence offsets, our findings indicate that SMGs undergoing strong interactions do not necessarily have more compact star-forming regions than the ones representing secular disks.

Based on our structural measurements, we investigate in the link between SMGs and passive galaxies, which are plausibly connected through the shut-down of star formation (referred to as ‘quenching’). In Figure 4, we plot the effective stellar sizes and resulting surface densities of our SMGs as a function of total stellar mass. As a reference sample for the passive galaxy population, we consider quiescent early-type galaxies at $z = 1.5$, as those might represent the ‘direct’ descendants of SMG once they have undergone quenching and evolved to the passive population within ~ 1 Gyr. Their sizes and surface densities are measured by van der Wel *et al.* (2014), who have quantified their R_e - M_* relation based on large samples. We further consider nearby massive early-type galaxies as their potential ultimate descendants in the local Universe (e.g. Toft *et al.* 2017).

The median stellar sizes and surface densities of our near-infrared bright SMGs are in good agreement with the quiescent population at $z = 1.5$ at the same stellar mass. Since

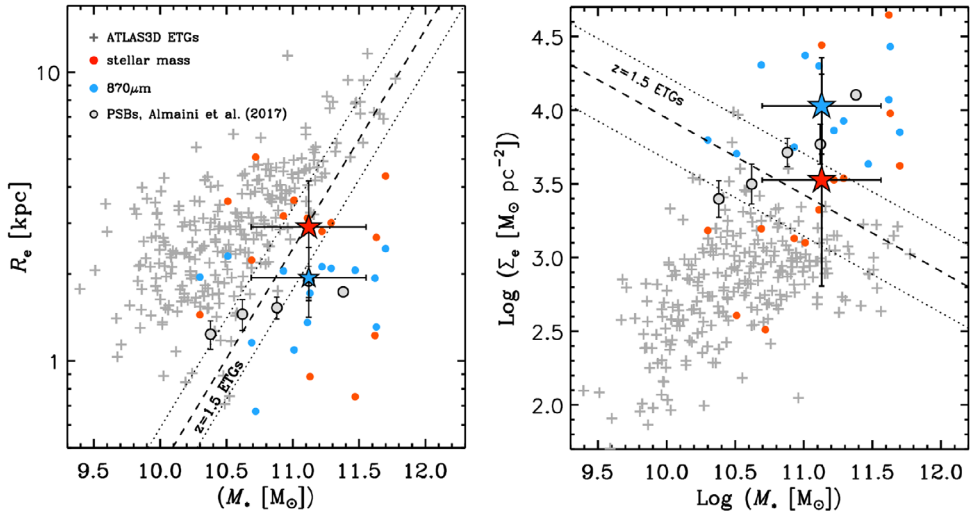


Figure 4. Comparison between the effective radii (left) and surface densities (right) of our SMG sample with local early-type galaxies from the ATLAS3D survey (Cappellari *et al.* 2011). The measurements of the submm and stellar components for our SMGs are shown as blue and red filled circles, respectively. Median values are indicated as stars. The stellar components of the underlying population of ATLAS3D galaxies are shown as gray crosses. The effective stellar sizes and surface densities of quiescent early-types at $z = 1.5$ from van der Wel *et al.* (2014) are shown as dashed lines, together with their scatter shown as dotted lines. Also shown are rest-frame optical sizes and surface densities of post-starburst galaxies (PSBs) at $1 < z < 2$.

the star-forming component is even more compact than the stars for our SMGs, those seem to fade into systems that represent the smaller and denser part of the quiescent galaxies at $z = 1.5$. Figure 4 also plots the effective sizes and resulting surface densities of post-starburst galaxies (i.e., systems selected to represent quiescent systems with very recent episodes of major star formation) at $1 < z < 2$ determined using rest-frame optical imaging by Almaini *et al.* (2017). The post-starburst systems exhibit on average effective sizes of 1.5–2 kpc within the stellar-mass range sampled by our SMGs, in agreement with a decrease in stellar size of SMGs before quenching. Thus, the post-starburst-phase might represent a link between the most immediate descendant of SMGs and the passive population at high redshift. The median stellar sizes and surface densities of our SMGs also occupy the locus of the most compact local ETGs that therefore might represent the ultimate descendants of SMG in the local Universe.

References

- Almaini, O., Wild, V., Maltby, D. T., *et al.* 2017, *MNRAS*, 472, 1401
 Bruzual, G. & Charlot, S. 2003, *MNRAS*, 344, 1000
 Cappellari, M., Emsellem, E., Krajnović, D., *et al.* 2011, *MNRAS*, 416, 1680
 Chen, C.-C., Smail, I., Swinbank, A. M., *et al.* 2015, *ApJ*, 799, 194
 Dekel, A., Birnboim, Y., Engel, G., *et al.* 2009, *Nature*, 457, 451
 Grogin, N. A., Kocevski, D. D., Faber, S. M., *et al.* 2011, *ApJs*, 197, 35
 Hayward, C. C., Kereš, D., Jonsson, P., *et al.* 2011, *ApJ*, 743, 159
 Hayward, C. C., Narayanan, D., Kereš, D., *et al.* 2013, *MNRAS*, 428, 2529
 Hodge, J. A., Karim, A., Smail, I., *et al.* 2013, *ApJ*, 768, 91
 Hodge, J. A., Swinbank, A. M., Simpson, J. M., *et al.* 2016, *ApJ*, 833, 103
 Hunt, L. K., Draine, B. T., Bianchi, S., *et al.* 2015, *A&A*, 576, A33
 Ikarashi, S., Ivison, R. J., Caputi, K. I., *et al.* 2015, *ApJ*, 810, 133
 Kim, D.-C., Evans, A. S., Vavilkin, T., *et al.* 2013, *ApJ*, 768, 102

- Koekemoer, A. M., Faber, S. M., Ferguson, H. C., *et al.* 2011, *ApJs*, 197, 36
- Lang, P., Schinnerer, E., Smail, I., *et al.* 2019, *ApJ*, 879, 54
- Miettinen, O., Delvecchio, I., Smolčić, V., *et al.* 2017, *A&A*, 606, A17
- Narayanan, D., Dey, A., Hayward, C. C., *et al.* 2010, *MNRAS*, 407, 1701
- Simpson, J. M., Smail, I., Swinbank, A. M., *et al.* 2015a, *ApJ*, 799, 81
- Stach, S. M., Smail, I., Swinbank, A. M., *et al.* 2018, *ApJ*, 860, 161
- Tadaki, K.-i., Genzel, R., Kodama, T., *et al.* 2017a, *ApJ*, 834, 135
- Toft, S., Zabl, J., Richard, J., *et al.* 2017, *Nature*, 546, 510
- van der Wel, A., Chang, Y.-Y., Bell, E. F., *et al.* 2014, *ApJL*, 792, L6
- Swinbank, *et al.* 2006, *MNRAS*, 371, 465
- Swinbank, A. M., Simpson, J. M., Smail, I., *et al.* 2014, *MNRAS*, 438, 1267
- Whitaker, K. E., Franx, M., Leja, J., *et al.* 2014, *ApJ*, 795, 104